Ase1/Prc1-dependent spindle elongation corrects merotely during anaphase in fission yeast

Thibault Courtheoux,[1,2] Guillaume Gay,[1,2] Yannick Gachet,[1,2] and Sylvie Tournier[1,2]

[1]Université de Toulouse and [2]Centre National de la Recherche Scientifique, Laboratoire de Biologie Cellulaire et Moléculaire du Controle de la Prolifération UMR5088, F-31062 Toulouse, France

Faithful segregation of sister chromatids requires the attachment of each kinetochore (Kt) to microtubules (MTs) that extend from opposite spindle poles. Merotelic Kt orientation is a Kt–MT misattachment in which a single Kt binds MTs from both spindle poles rather than just one. Genetic induction of merotelic Kt attachment during anaphase in fission yeast resulted in intra-Kt stretching followed by either correction or Kt disruption. Laser ablation of spindle MTs revealed that intra-Kt stretching and merotelic correction were dependent on MT forces. The presence of multiple merotelic chromosomes linearly antagonized the spindle elongation rate, and this phenomenon could be solved numerically using a simple force balance model. Based on the predictions of our mechanical model, we provide in vivo evidence that correction of merotelic attachment in anaphase is tension dependent and requires an Ase1/Prc1-dependent mechanism that prevents spindle collapse and thus asymmetric division and/or the appearance of the cut phenotype.

Introduction

The fidelity of kinetochore (Kt) attachment during mitosis is essential to maintain genetic integrity in all eukaryotes. Studies in mammalian tissue culture cells suggest that Kt–microtubule (MT) misattachments are a major cause of chromosome missegregation and aneuploidy (Cimini et al., 2001, 2003). Merotelic Kt orientation is a Kt–MT misattachment in which a single Kt binds MTs from both spindle poles rather than just one. Such misattachments occur frequently during vertebrate early development (Cimini et al., 2003) and are not detected by the spindle assembly checkpoint (SAC; Khodjakov et al., 1997; Wise and Brinkley, 1997; Cimini et al., 2004). Rather, merotelic attachments are corrected before anaphase onset by an aurora B–dependent mechanism that promotes MT destabilization (Cimini et al., 2006). Therefore, promoting Kt–MT turnover appears to be the key to correcting merotelic attachment. A recent study established a direct link between the presence of extra centrosomes, the accumulation of lagging chromosomes, and chromosomal instability (Ganem et al., 2009). However, the precise mechanisms leading to the appearance of aneuploidy in cancer cells are still unknown.

Model organisms such as yeast have proven to be powerful tools in which to study the mechanisms that control chromosome attachment. In budding yeast, a single MT attachment site is present on each Kt (O'Toole et al., 1999), making it impossible to study merotelic attachment directly. However, spindle elongation was shown to be delayed in the presence of dicentric chromosomes (Gardner et al., 2008). Fission yeast, like higher eukaryotes, possesses multiple MT attachment sites on each Kt (Ding et al., 1993). Sister chromatid cohesion is mediated by a conserved protein complex known as cohesin (Uhlmann et al., 1999). Centromeric heterochromatin attracts cohesin, thereby ensuring sister centromere cohesion and proper chromosome segregation (Sakuno et al., 2009). The Pcs1/Mde4 monopolin complex proteins maintain MT-binding sites together in the central Kt domain (Gregan et al. 2007), whereas the centromeric heterochromatin coating the flanking domains provides rigidity, both systems contributing to the prevention of merotely (Gregan et al., 2007). Surprisingly, the monopolin complex also appears to be required to promote spindle elongation and integrity

T. Courtheoux and G. Gay contributed equally to this paper.

Correspondence to Sylvie Tournier: tournier@cict.fr; or Yannick Gachet: gachet@cict.fr

Abbreviations used in this paper: Kt, kinetochore; MT, microtubule; SAC, spindle assembly checkpoint; SPB, spindle pole body; wt, wild type.

The Rockefeller University Press $30.00
J. Cell Biol. Vol. 187 No. 3 399–412
www.jcb.org/cgi/doi/10.1083/jcb.200902093

(Choi et al., 2009). It is currently accepted that in *Schizosaccharomyces pombe*, spindle elongation is determined by the speed of tubulin incorporation at the spindle midzone (Mallavarapu et al., 1999) rather than by the pushing forces of astral MTs in anaphase B (Tolić-Nørrelykke et al., 2004). The spindle MT midzone is organized by the MT-bundling protein Ase1 (also known as Prc1; Pellman et al., 1995; Loïodice et al., 2005; Yamashita et al., 2005). It is presently unknown whether the spindle elongation defect seen in monopolin mutants is caused by the presence of lagging chromosomes as previously suggested in cohesion mutants (Pidoux et al., 2000).

Because of the complexity of the mechanisms controlling spindle morphogenesis, mathematical and computational models that integrate experimental results have been developed over the past few years (Gardner and Odde, 2006; Mogilner et al., 2006). These can be used to predict mitotic phenotypes or to simply verify biological assumptions. In our study, we genetically induced merotely in fission yeast and quantitatively characterized its impact on mitotic progression from metaphase to anaphase, cytokinesis, and cell abscission. Using live cell video microscopy and laser surgery of merotelic Kts, we formally demonstrate that merotelic Kt stretching is specifically mediated by a tension-dependent mechanism exerted by MTs. Using a mathematical model of merotelic attachment, we find that mitotic progression can be mechanically blocked by Kt misattachment independently of the SAC. Based on the predictions of our mechanical model, we provide in vivo evidence that the function of the interdigitated pole–pole spindle MTs, which support spindle structure and provide tension across the spindle, participate in the correction of merotelic attachment in anaphase and prevent the appearance of the cut phenotype and asymmetric division.

Results

Merotelic attachment can be corrected during anaphase B in fission yeast

Based on previous data suggesting that centromeric cohesion is required to prevent merotelic attachment (Gregan et al., 2007), we characterized the segregation defects seen in cells mutated for the Rad21 cohesin subunit at the permissive temperature of 25°C. We analyzed Kt dynamics during metaphase in either wild-type (wt; Fig. 1 A) or *rad21-K1* cells (Fig. 1 B). The movements of the six Kts were recorded (Fig. 1, A and B, top; and Videos 1 and 2), and automated analysis was used to map the position of each Kt relative to the spindle pole bodies (SPBs) for each frame of the video (Fig. 1, A and B, bottom; see Materials and methods). Using this methodology, it was possible to determine the number of Kts present at each SPB for each frame of the video. This number is reported along the top of the kymograph using a color code (Fig. 1, A and B, middle). In wt cells, the six Kts make rapid oscillatory movements between the spindle poles during metaphase and congress into two bunches of three on either side of the spindle midzone before the onset of anaphase A as previously described (Fig. 1 A; Tournier et al., 2004; Courtheoux et al., 2007). Migration of the Kts to the poles is coordinated; i.e., all of the Kts arrive at the poles within 30 s. By filming a *rad21-K1 ndc80-gfp cdc11-cfp* strain to simultaneously image both poles and Kts from metaphase to anaphase, we confirmed that the stretched Kts in this strain were indeed single sister chromatids. In the kymograph representation in Fig. 1 B (middle), it is possible to visualize individual Kts (a maximum of six in fission yeast) at different time points before Kt stretching (Video 2). At the 90-s time point, three Kts are located at the top pole, whereas 40 s later, two others have arrived at the bottom pole (Fig. 1 B, middle), leaving a single, stretched merotelic Kt in the middle. We confirmed that stretched Kts were single chromatids using a strain that allows simultaneous observation of both the centromere of chromosome I (two red dots after chromosome replication) and the Kts (six green dots; Fig. S1). This finding was further confirmed by filming cells in the presence of Hoechst and quantifying the fluorescence intensity (Fig. S1, D and E).

22% of mitotic cells ($n = 79$) showed stretched merotelic Kts (Fig. 1 C). By following the merotelic Kt with time, we found that at least 75% ($n = 17$) of these relaxed into a single dot, which segregated to one of the poles (see Fig. 5 B). In no case did the presence of a merotelic attachment lead to the cut phenotype, suggesting that most merotelic Kts are corrected (Fig. 1 D). This was confirmed in fixed mitotic cells in which only 3% of cells ($n = 1{,}966$) showed a "cut-like" phenotype (as judged by the presence of DAPI signal under calcofluor-stained septum). The 25% of stretched merotelic Kts that were not corrected instead disrupted into two pieces that regained the two poles (Fig. 1 B, 450 s). The mean maximum stretching distance of a Kt before its disruption was 1.56 ± 0.28 µm ($n = 7$).

Collectively, these observations demonstrate that the stretched lagging chromosomes, which are often observed during mitosis in *rad21-K1* cells at the permissive temperature, are merotelic. Most importantly, such merotelic attachments are corrected during anaphase.

Kt stretching during merotelic attachment is imposed by MT-dependent forces

To investigate whether Kt stretching was dependent on forces imposed by spindle MTs on the merotelic Kt, we performed laser ablation experiments on spindles showing a single, stretched Kt (Botvinick et al., 2004). We used a 2D-guided pulsed Nd:YAG laser ($\lambda = 532$ nm) to perform multiple spindle ablation simultaneously (see Materials and methods) on cells expressing an α2-GFP tubulin (Fig. S1 F). To control for laser-cutting efficiency, we mixed an α2-GFP tubulin strain (Fig. 2 A, control) and a *rad21-K1 ndc80-gfp cdc11-cfp* strain (Fig. 2 A, merotelic Kt) and simultaneously performed laser ablation in both populations (Video 3). In control cells, laser ablation resulted in the collapse of decorated spindles (Fig. 2 A, top), suggesting that the settings used were sufficient to disrupt spindle MTs. When laser ablation was performed on spindles with merotelic chromosomes, the stretched Kt immediately relaxed and moved toward the pole opposite to the cut (Fig. 2 A, bottom). Kymographic analysis of Kt dynamics during laser ablation is presented in Fig. 2 B. In all cases ($n = 37$), the stretched Kt relaxed to a single dot which then moved, in 75% of cases, to the pole opposite to the cut. The speed at which Kts regained the pole (1.15 ± 0.36 µm/min; $n = 11$)

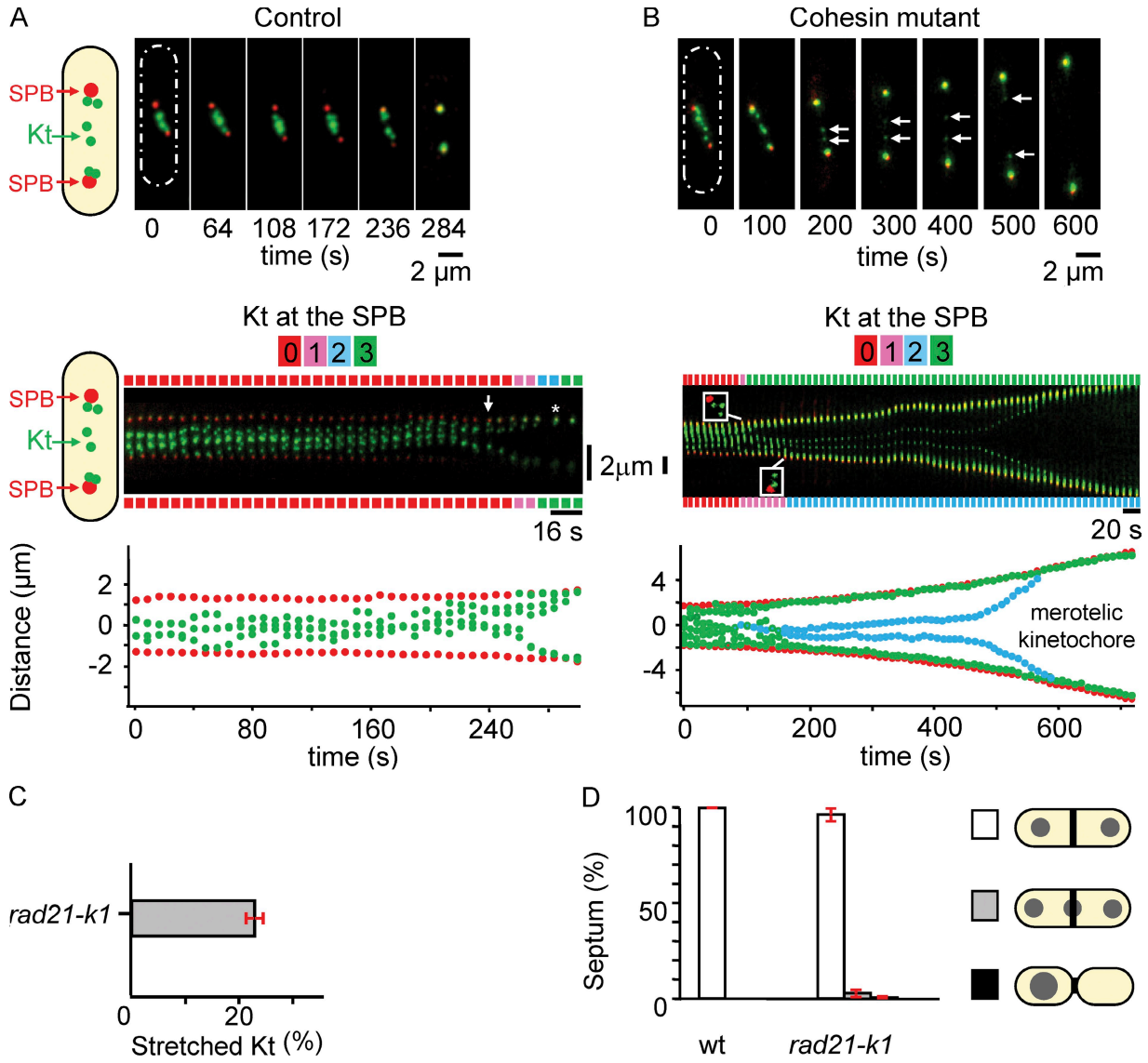

Figure 1. **A defect in centromeric cohesion affects Kt biorientation.** (A and B, top) Image series showing an *ndc80-gfp cdc11-cfp* cell (A) or a *rad21-K1 ndc80-gfp cdc11-cfp* cell (B) during mitosis. The six Kts (green) are located between the two SPBs (red). Schematic representations of fission yeast cell shape are shown (dashed ovals). (middle) Kymograph of the cell shown above. In control cells, anaphase A (arrows) takes place ~45 s before anaphase B (asterisk). The number of Kts at each SPB is indicated for each time point on both sides of the kymograph. (bottom) Automated tracking analysis of SPB (red) and Kt (green) positions in the same cell (see Materials and methods). (C) Percentage of mitotic cells with stretched merotelic Kts in *rad21-K1 ndc80-gfp cdc11-cfp* cells (*rad21-K1*). (D) Percentage of cut-like phenotype and asymmetric cells in wt (n = 2,466) and *rad21-K1* cells (n = 1,966) stained with DAPI calcofluor. White, correct segregation with a septum; gray, cut cells; black, asymmetrically dividing cells. Error bars indicate SD.

was similar to that observed for the poleward movement of Kts during anaphase (Fig. 2 B). These experiments demonstrate that merotelic Kts are subjected to opposed forces generated by spindle MTs and that merotelic Kt correction during anaphase is dependent on the destabilization of MTs.

Merotelic attachment linearly reduces spindle elongation rate

It was previously reported that the presence of lagging chromosomes in fission yeast affects the rate of spindle elongation during anaphase B (Pidoux et al., 2000). Because several categories of lagging chromosomes were observed in this study, it was unclear whether the effect on spindle elongation was imposed by merotelic as opposed to monotelic (chromosome attached to a single pole) attachment. Nevertheless, Pidoux et al. (2000) suggested that the negative effect of merotelic attachment on spindle elongation was caused by the activation of a checkpoint rather than the result of mechanical restraint. Therefore, we investigated whether the presence of additional merotelic chromosomes affected the rate of anaphase B. Automated analysis of videos of *rad21-K1* cells containing one (Fig. 1 B and Fig. 3 A) to three merotelic attachments (Fig. S2, A and B) revealed a linear reduction of spindle elongation rate from 1.3 ± 0.09 µm/min (n = 12) in control cells to 0.123 ± 0.06 µm/min (n = 5) in the presence of three merotelic attachments (Fig. 3 B).

To confirm that merotelic attachment directly antagonizes anaphase B, we followed the changes in spindle elongation rate in cells exhibiting Kt disruption. As shown in Fig. 3 (A and C),

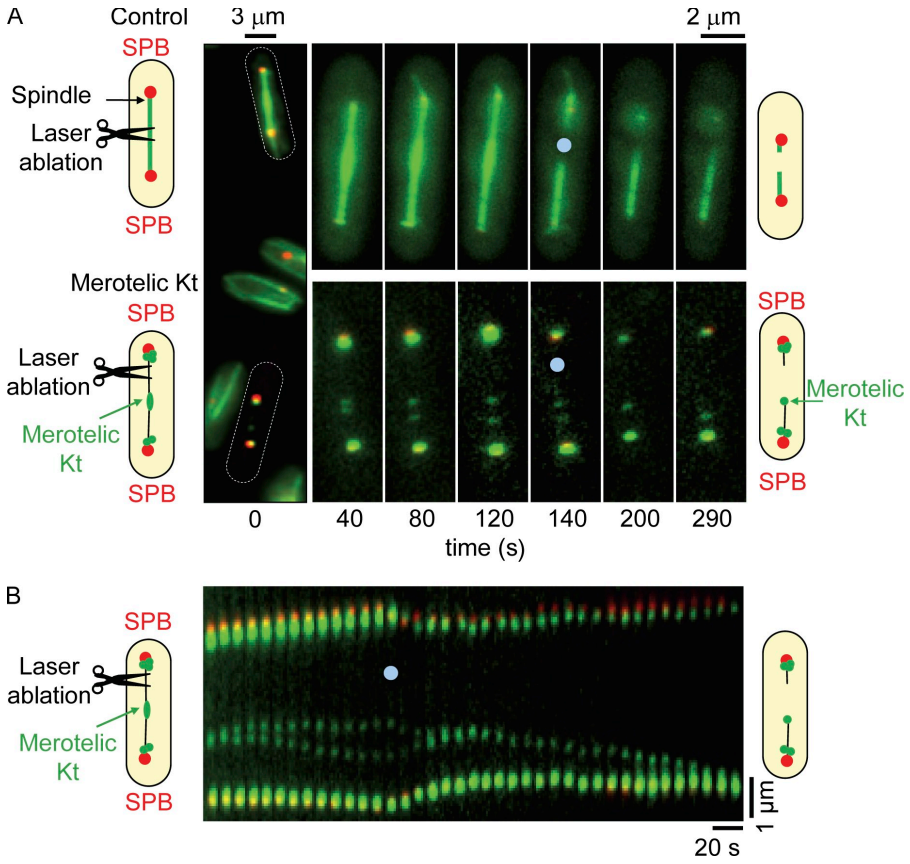

Figure 2. **Kt stretching is imposed by MT-dependent forces.** (A) A mixed population of *atb2-gfp cdc11-cfp* (control) and *rad21-K1 ndc80gfp cdc11-cfp* cells (merotelic Kt) was treated simultaneously by laser ablation. Image series showing the two cells before (time 0) and at the moment of laser ablation (see Materials and methods). Schematic representations of fission yeast cell shape are shown (dashed ovals). (B) Kymograph of the *rad21-K1* cell shown in A illustrating the relaxation of the merotelic Kt after laser ablation. Blue dots indicate the point of laser impact.

anaphase B increased more than twofold (0.95 ± 0.03 to 2.19 µm/min; $n = 7$) after the disruption of a single, stretched Kt. These experiments show that merotelic attachments directly and incrementally reduce spindle elongation.

Merotelic attachment leads to spindle collapse in the absence of the bundling factor Ase1

Spindle elongation requires the activity of motor proteins at the interdigitated MT midzone, the organization of which involves the antiparallel bundling protein Ase1 (also known as Prc1; Pellman et al., 1995; Loïodice et al., 2005; Yamashita et al., 2005). In fission yeast, *ase1Δ* cells enter anaphase but fail to complete anaphase B (Loïodice et al., 2005). To investigate the role of overlapping MTs on mitotic progression in the presence of merotelic attachment, we analyzed *ase1Δ* cells with a merotelic attachment (Fig. 4 A). The double mutant *ase1Δ rad21-K1* was inviable at the semipermissive temperature (31–33°C), although both single mutants were alive at these temperatures (Fig. S4 B). At the permissive temperature (25°C), however, cells entered mitosis in the presence of a stretched merotelic Kt. However, during midanaphase B, the spindle collapsed, and the distance between the two SPBs rapidly diminished (from 7 to 2 µm; rate = −1.05 ± 0.1 µm/min; $n = 6$; Fig. 4 A). Spindle collapse at this rate was never observed in the two single mutants. We confirmed this result by visualizing simultaneously both MTs (α-tubulin GFP) and the merotelic Kt (Ndc80-GFP). Initiation of anaphase B in *ase1Δ* was followed by the disassembly of the spindle and the two SPBs becoming symmetrically positioned within the cell (Fig. 4 B, left; and Video 4). In the presence of a merotelic Kt, however, a general plus end MT depolymerization lead to spindle collapse at a rapid rate (Fig. 4 B, right; and Video 5). These experiments demonstrate that merotelic attachment can lead to spindle collapse when the structure of the spindle is compromised.

Ase1/Prc1/Map65 participates in the correction of merotelic attachment in anaphase and prevents the appearance of cut phenotype and asymmetric division

It has previously been reported that lagging chromosomes can affect cell abscission (completion of cytokinesis; Norden et al., 2006). However, experiments in fission yeast suggest that no coordination exists between chromosome segregation and cytokinesis, as *cut* mutants complete cytokinesis in the absence of chromosome segregation (Yanagida, 1998). If this is the case, it is likely that correction of merotelic attachment in anaphase will be essential to prevent the appearance of a cut phenotype and subsequent cell death. To investigate this point further, we performed live cell imaging and followed merotelic attachment from early mitosis to cytokinesis by observing Kt dynamics and cytokinetic actin ring contraction simultaneously within the same cell using the strain *ndc80-gfp* (Kt) *cdc11-cfp* (SPBs) *myo2-gfp* (actomyosin ring; Fig. 5; Mulvihill et al., 2001). In control cells, Kt segregation and spindle elongation were completed before myosin II ring contraction (Fig. 5 A and Video 6). The same experiment performed in a cohesion mutant background revealed that the majority of stretched merotelic Kts

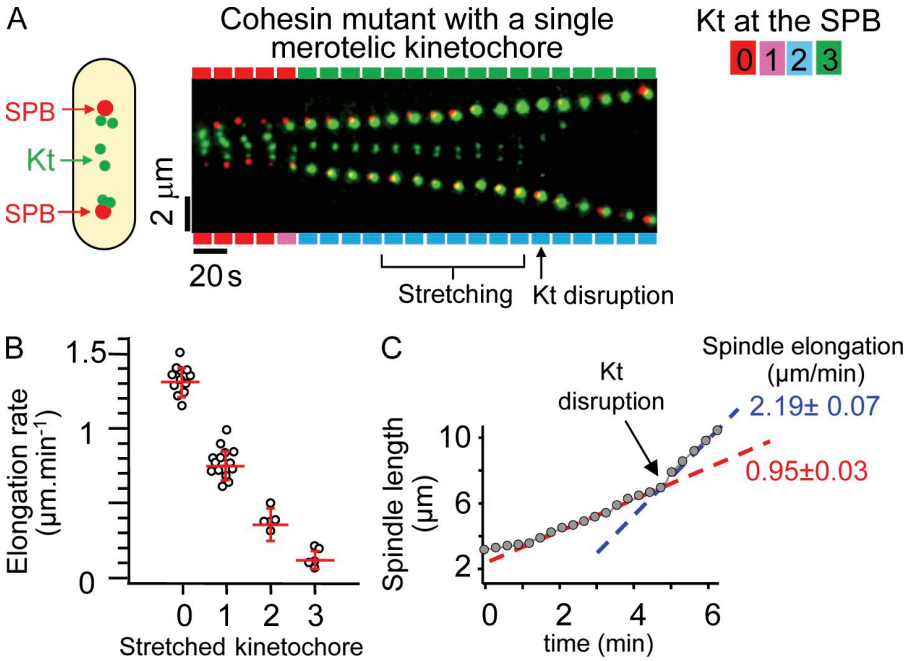

Figure 3. **Merotelic attachment influences the rate of spindle elongation.** (A) Kymograph of a *rad21-K1 ndc80-gfp cdc11-cfp* cell showing a single, stretched Kt. (B) Spindle elongation rate of *rad21-K1 cdc11-cfp ndc80-gfp* cells in the absence of merotelic attachment (zero) or in presence of one, two, or three merotelic Kts. (C) Graphic representation of spindle elongation in the *rad21-K1 ndc80-gfp cdc11-gfp* cell shown in A (red dots). The rate of spindle elongation was calculated before (red) or after (blue) disruption of the merotelic Kt. Error bars indicate SD.

(85%; $n = 43$) were corrected during anaphase B before completion of actomyosin ring contraction (Fig. 5 B and Video 7), whereas the remaining 15% were disrupted into two pieces. Oppositely, when tension across the spindle was defective (*ase1Δ*; Fig. 5, C and D; and Videos 8 and 9), only 34% ($n = 20$) of merotelic attachments were corrected and 6% of stretched merotelic Kts ($n = 20$) disrupted into two pieces. Instead, we found that merotelic attachment in the absence of Ase1 lead to either

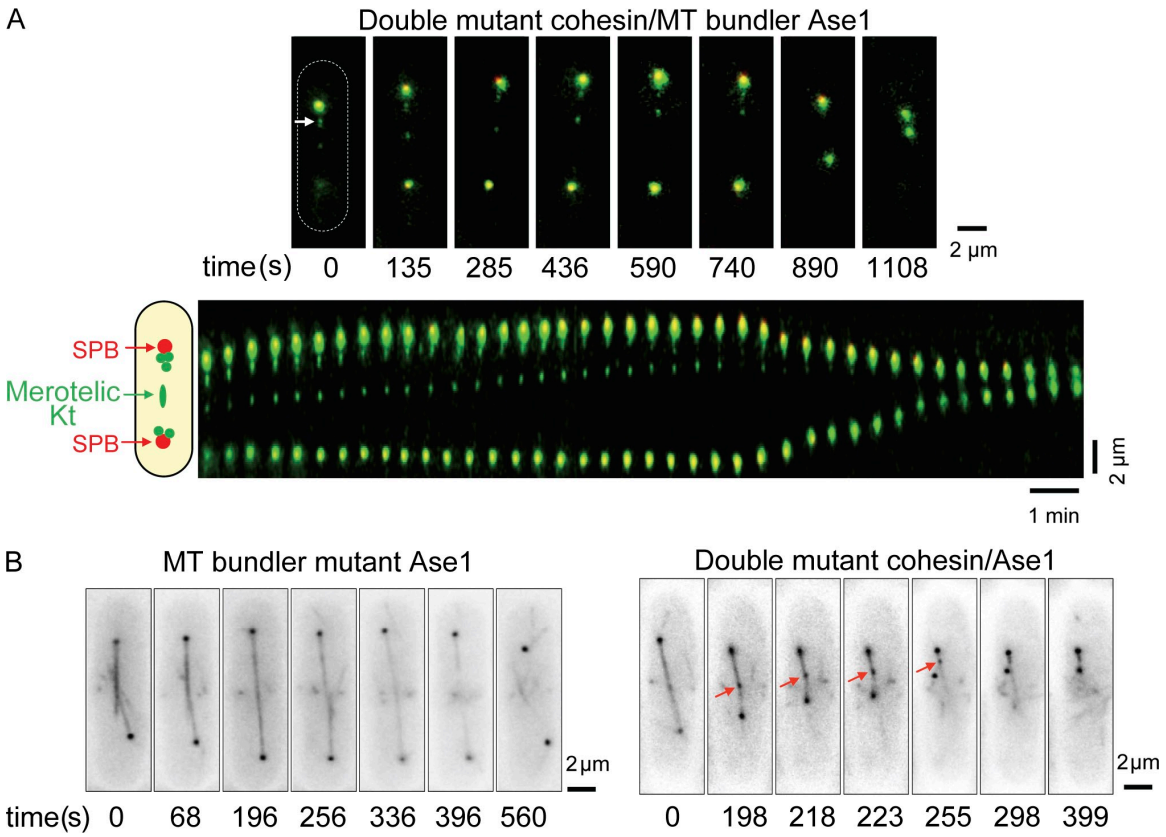

Figure 4. **Merotelic attachment leads to abortive anaphase when interdigitated MTs are defective.** (A, top) Image series of a *rad21-K1 ase1Δ ndc80-gfp cdc11-cfp* cell during mitosis showing two lagging Kts (one of them stretched; white arrow). (bottom) Kymograph showing a rapid collapse of the spindle. A schematic representation of a fission yeast cell shape is shown (dashed oval). (B, left) Image series of *ase1Δ atb2-gfp* (MTs) *ndc80-gfp* (Kts) during mitosis. (right) Image series of *rad21-K1 ase1Δ SV40-gfp-atb2* (MTs) *ndc80-gfp* (Kts) cell during mitosis in the presence of a merotelic attachment (red arrows).

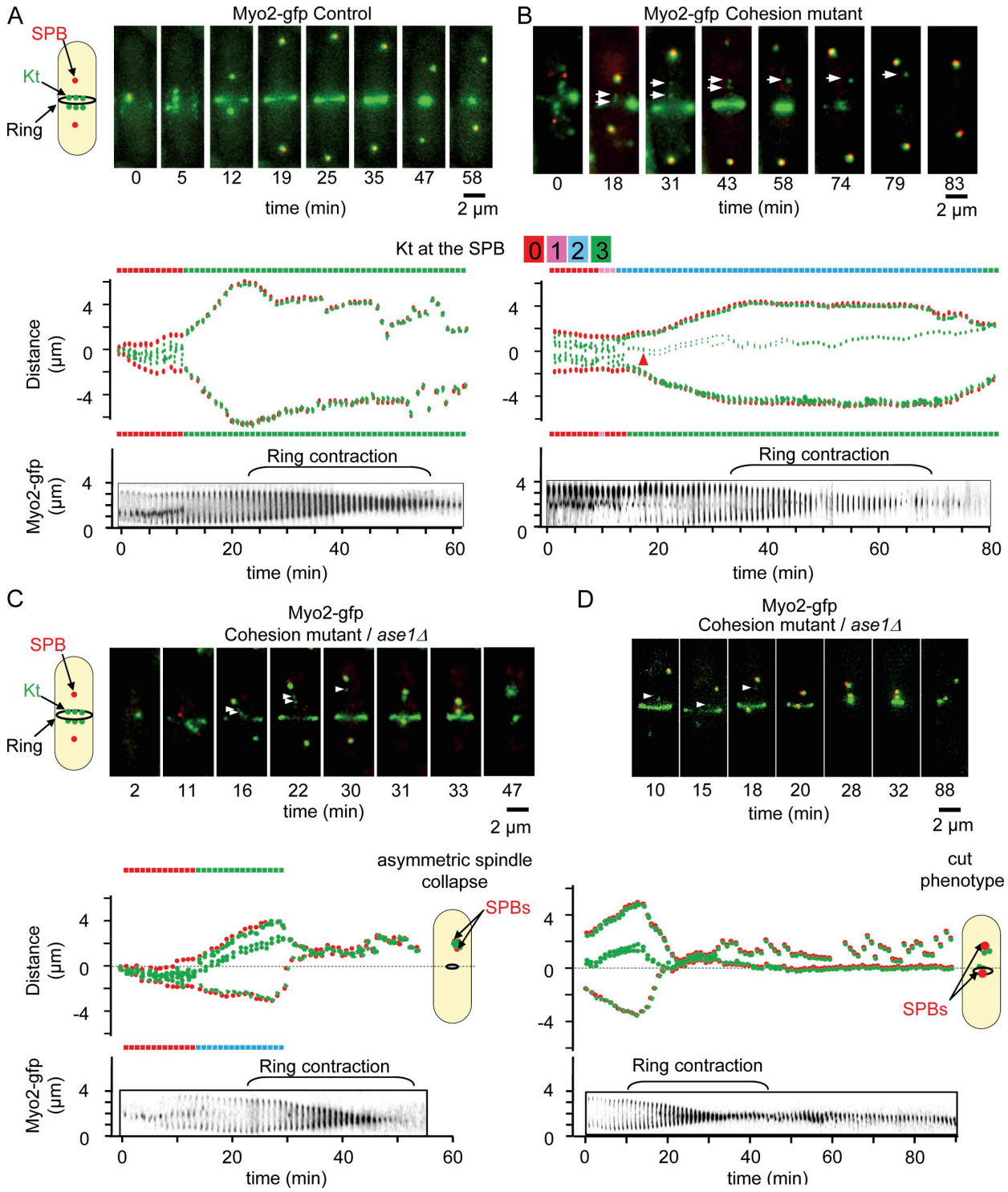

Figure 5. **Merotelic attachment leads to the cut phenotype and asymmetric division when interdigitated MTs are defective.** (A–D, top) Image series showing an *ndc80-gfp cdc11-cfp myo2-gfp* cell (A), a *rad21-K1 ndc80-gfp cdc11-cfp myo2-gfp* cell (B), or an *ase1Δ rad21-K1 ndc80-gfp cdc11-cfp myo2-gfp* cell (C and D) during mitosis from metaphase to anaphase up to cytokinesis. The six Kts (green) are located between the two SPBs (red) with the actomyosin ring located at the midzone. (middle) Automated tracking analysis of the cell shown above. The number of Kts at each SPB is indicated for each time point on both sides of the kymograph. Kt dynamics (middle) and cytokinesis (bottom, ring contraction) were filmed simultaneously. Arrowheads indicate the positions of the stretched merotelic Kts. (B) After correction (43 min), the Kt moves to the SPB, and cytokinesis takes place. (C) Example of an asymmetric spindle collapse in an *ase1Δ* mutant in the presence of a merotelic attachment. After completion of cytokinesis, the formation of an anucleate cell and a diploid cell is observed. (D) Example of a symmetric spindle collapse seen in an *ase1* mutant in the presence of merotelic attachment. After the execution of cytokinesis, the formation of a cut phenotype is observed.

asymmetric (40%; $n = 20$; Fig. 5 C and Video 8) or symmetric spindle collapse (20%; $n = 20$; Fig. 6 D and Video 9). In such situations, ring contraction and cell abscission took place normally, leading to the appearance of either cut cells (Samejima et al., 1993) or asymmetric division followed by cell death (Fig. 5, C and D; Fig. S3; and see Fig. 8). These findings were confirmed in fixed cells (Fig. S4 A). In agreement with these results, *ase1Δ* was synthetically lethal with *rad21-K1* at the semipermissive temperature (31–33°C), although the single mutants were alive at these temperatures, confirming that Ase1/Prc1 participates in the correction of merotelic attachment in anaphase cells (Fig. S4 B). Collectively, these experiments demonstrate that correction of merotelic Kt during anaphase B is triggered by an Ase1/Prc1-dependent tension mechanism.

A minimal mechanical model predicts that merotelic attachments mechanically block spindle elongation and cause mitotic regression

To validate our in vivo observations, we established a simple mathematical model based on a framework previously described (Brust-Mascher et al., 2004; Gardner et al., 2005; Civelekoglu-Scholey et al., 2006). In our model, the mitotic spindle is defined by four objects, the two faces of the merotelic Kt and the two SPBs (Fig. 6 A). Because fission yeast possesses up to four Kt–MT attachment sites per chromosome (Ding et al., 1993), our model assumes a maximum of four MTs attached per Kt distributed on each side of the spindle. The set of 10 parameters required to generate this model was obtained by direct measurements of in vivo characteristics such as Kt speed at anaphase onset, spindle elongation rate, and merotelic Kt mean stretching length. To determine the stiffness and friction coefficient of the merotelic Kt, we performed a double-laser ablation experiment in which both sides of the merotelic Kt were cut (Fig. 6 C, left). From the observed relaxation of the system, we were able to determine precisely the stiffness and friction coefficient of the merotelic Kt (Fig. 6 C, right). This set of values was then maintained throughout the study (Table I).

Fig. 6 D shows a simulation of a single merotelic attachment that is undergoing stretching. The number of MTs attached to the merotelic Kt is indicated on each side of the graph. This model was sufficient to reproduce the in vivo dynamics of the merotelic Kt and could be applied to both two (Fig. S5 A) and three (Fig. S5 B) merotelic attachments. The final setting of the model reproduced the relationship between spindle elongation rate and the number of merotelic Kts present within the spindle (Fig. 6 E). We were able to validate our model by determining the effect of double-laser ablation in silico on both sides of the merotelic Kt (Fig. 6 F, left). Kymograph analysis of this experiment, coupled with convolution of the signal, is presented in Fig. 6 F (middle and right), revealing that the friction coefficient of the merotelic Kt determined in silico is similar to that observed in vivo. We tested the effect of multiple merotelic attachments on mitotic progression. Simulations predicted that more than three merotelic attachments would result in a negative spindle elongation rate (i.e., spindle collapse) at a speed of 0.2 ± 0.11 μm/min ($n = 18$). These findings suggest that our model could be used to predict complex phenotypes associated with merotelic attachment.

In conclusion, our results showed that in presence of merotelic attachment, the spindle behaves as a nanomachine, whose behavior can be numerically described using a simple force balance model. We further demonstrate that merotelic attachment can mechanically block spindle elongation and cause spindle regression.

In silico evidence that merotelic attachment leads to spindle collapse in the absence of interdigitated MTs

To validate our in vivo observations, we abrogated the pushing force present in between the two SPBs in the mechanical model at the 80-s time point (Fig. 7 A, right). In this situation, merotelic Kts were still able to stretch but failed to disrupt as a result of the lack of tension exerted on the Kt (unpublished data). Instead, we observed the immediate collapse of the spindle at a rapid negative rate of -1.47 ± 0.35 μm/min ($n = 10$; Fig. 7 B). Thus, our mechanical model predicts that the mitotic spindle will rapidly collapse in the presence of a merotelic Kt when interdigitated MTs are absent or weak and that proper tension across the spindle underlies Kt correction and disruption during anaphase B. An alternative mathematical model to reproduce the *ase1* mutant phenotype would be to reduce the pushing force as the spindle elongates until a critical length of 7 μm in which the force is reduced to zero. A similar result was obtained in this type of simulation (Fig. S5, C and D). These experiments validate the prediction of our merotelic model, demonstrate that merotelic attachment can lead to spindle collapse when the structure of the spindle is compromised, and confirm that correction of merotelic Kts during anaphase B is triggered by a tension-dependent mechanism.

Discussion

The maintenance of genetic stability is essential to prevent the development of human cancers. Genetic instability can be caused by several mechanisms such as a defective DNA damage checkpoint or a defect in chromosome segregation, which is also called aneuploidy. Although aneuploidy is a well-described phenotype of solid tumors, the molecular mechanisms involved in this process are controversial. Some evidence suggests that aneuploidy can be induced by a failure in mitotic control (Cahill et al., 1998). Indeed, it is well established that defects in MT–Kt attachment activate the SAC (Cleveland et al., 2003). However, recent studies suggest that aneuploidy can be induced even in the presence of a robust checkpoint (Tighe et al., 2001; Thompson and Compton, 2008). Perhaps the SAC does not detect all types of Kt misattachment. Indeed, several studies suggest that the SAC is not activated in the presence of merotelic attachment and that, consequently, this misattachment does not affect mitotic progression (Cimini et al., 2001, 2004).

Cohesion between sister chromosomes is mediated by a protein complex degraded in mitosis by a protease called separase (Tatebayashi et al., 1998; Tomonaga et al., 2000; Nasmyth and Schleiffer, 2004). Recent work in *S. pombe* revealed that

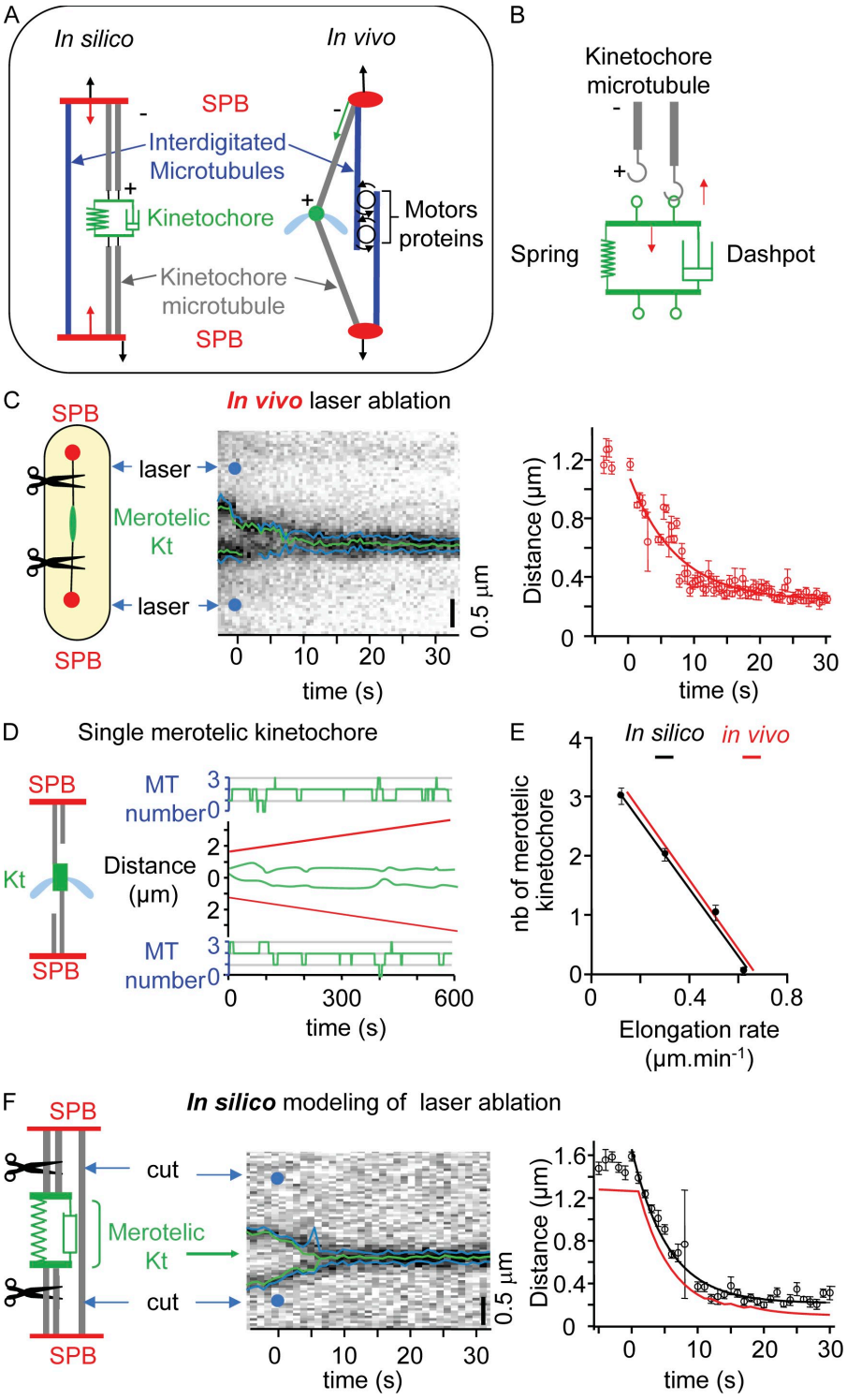

Figure 6. **A minimal model for the description of merotelic attachment.** (A, left) Schematic representation of the fission yeast spindle. MTs and associated proteins are symbolized by force generators fixed to the two SPBs; Kt force generators (red arrows) apply forces between the Kt and the poles, whereas spindle force generators (black arrows) apply forces between both SPBs. (B) In the mechanical model, the Kt is composed of a spring and a dashpot, and each Kt provides a site for MT (gray) attachment (green loop). Red arrows indicate the forces applied by the attached MT (upward arrow) and the Kt elastic structure (downward arrow). (C) Characterization of the merotelic Kt spring constant using laser ablation. (left) Laser ablation on both sides of the merotelic Kt is performed. (middle) Kymograph of the merotelic Kt after laser ablation (blue dots). (right) Graphic representation showing Kt relaxation after laser ablation (time 0 = time of laser impact). (D) Simulation of mitotic progression in the presence of a single merotelic Kt (green), with SPBs shown in red. The number of MTs attached to the Kt is indicated for each SPB (green). (E) Comparison of spindle elongation rates between simulated (black) and in vivo data (red) as a function of the number (nb) of merotelic Kts. (F, left) Kt and spindle force generators are shut off (virtual laser ablation) during a merotelic simulation. (middle) Synthetic kymograph of a merotelic Kt after the elimination of the two force generators (blue dots). (right) Comparison of Kt relaxation between simulated (black) and in vivo data (red). Error bars indicate SD.

cohesins are key elements, which determine the type of MT–Kt attachment (Toyoda et al., 2002; Yokobayashi et al., 2003; Sakuno et al., 2009). Indeed, alteration of mitotic cohesin with a thermosensitive mutant (*rad21-K1*) results in severe chromosome segregation defects and leads to activation of the SAC at the nonpermissive temperature (Tatebayashi et al., 1998; Toyoda et al., 2002). However, at the permissive temperature of 25°C, the *rad21-K1* mutant is able to form a bipolar spindle and initiates mitosis in the absence of chromosome alignment, as previously reported in cohesin-depleted *Xenopus laevis* extracts (Kenney and Heald, 2006). Several other studies suggest that a lack of cohesion induces segregation defects compatible with merotelic attachment (Kenney and Heald, 2006; Gregan et al., 2007), suggesting that cohesin may play a structural role in Kt–MT attachment. In our study, we formally demonstrate that the cohesin Rad21 is required to prevent the formation of merotelic attachment. We also show that merotelic attachment leads to intra-Kt stretching, which is abolished by laser Mt ablation.

Table I. **Parameters used in the merotelic model**

Notation	Definition	Adimensionalized value	Value
General			
N	Number of merotelic Kts	1–4	NA
M_k	Maximum number of Kt–MTs per side	4	NA
Geometry			
L_0	Spindle initial length	2–6	2–6 µm
d_o	Equilibrium distance between attachment sites	0.01	0.01 µm
Mechanical			
κ	Centromere spring constant	2	20 *pN*/µm
μ_s	SPB friction coefficient	1.4	420 *pN.s*/µm
μ_k	Centromere friction coefficient	1	300 *pN.s*/µm
μ_c	Sister chromatid friction coefficient	0.2	60 *pN.s*/µm
Motors			
F_k	Kt force generators stall force	1	10 *pN*
V_k	Kt force generators maximum speed	1	310^{-2} µm/*s*
F_{mz}	Midzone force generators stall force	7	70 *pN*
V_{mz}	Midzone force generators maximum speed	0.4	1.210^{-2} µm/*s*
Dynamic instability			
f_a	Attachment frequency	0.04	0.04 1/*s*
f_d	Detachment frequency	0.1	0.1 1/*s*

NA, not applicable. Value is determined with F_k at 10 *pN* and V_k at 0.03 µm/*s*.

Most importantly, we also observed stretching and disruption of merotelic Kt in cohesin-plus background strains, although these events were rare (unpublished data). Recent work has highlighted the importance of intra- as opposed to inter-Kt stretching in satisfying the SAC (Maresca and Salmon, 2009; Uchida et al., 2009). It is likely that motor proteins are required in fission yeast to stretch merotelic Kts, and our model provides a unique system to identify which mitotic players are required for the establishment of tension across the merotelic Kt.

The aurora B kinase plays a critical role in correcting Kt misattachment by phosphorylating key substrates at the Kt and promoting the turnover of Kt MTs (Tanaka et al., 2002; Cimini et al., 2006). It has been proposed that the physical distance between aurora B and its Kt substrates determines whether MT–Kt connections are maintained (Tanaka et al., 2002; Andrews et al., 2004). We found that the unique *S. pombe* aurora kinase, Ark1, was present on the outer faces of stretched merotelic Kts during anaphase, although the signal seen in anaphase was considerably weaker than during metaphase (unpublished data). Based on these observations, the simplest interpretation of our findings is that the anaphase correction of merotelic attachment is aurora independent. An alternative mechanism is that unbalanced forces across the merotelic Kt participate in the correction mechanism in anaphase. Further experiments will be necessary to clarify the participation of aurora in anaphase B.

Although it was previously suggested that merotelic attachment does not affect mitotic progression, we demonstrate in this study that spindle elongation rate is linearly dependent on the number of merotelic Kts. This effect is independent of the SAC, as deletion of either Mad2 or Bub1 does not prevent the appearance of this phenotype (unpublished data). In agreement with this finding, we found that Mad2 was never recruited onto merotelic Kts in anaphase (unpublished data). In many respects, our in vivo results are similar to what is seen in vitro in *Xenopus* egg extracts where bipolar spindles assemble in the absence of either chromosomes or centrosomes, suggesting that spindle morphogenesis is solely dependent on the presence of motor proteins (Heald et al., 1996).

Multiple proteins are involved in the structure of the Kt, and several of them are known to influence MT dynamics. An advanced mathematical model reproducing the biochemical properties of each Kt component is the ultimate goal, although

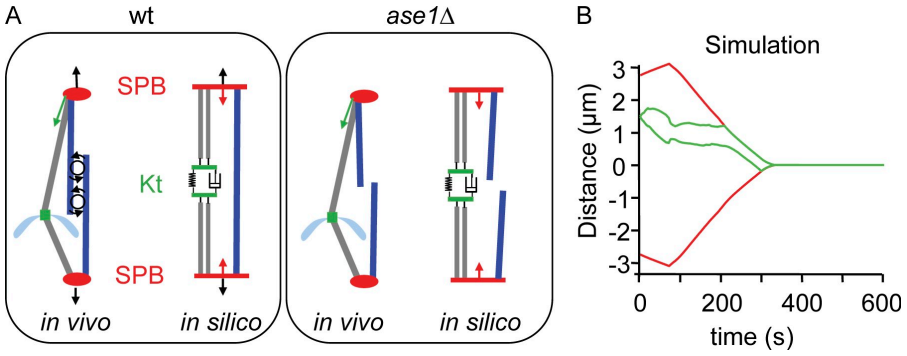

Figure 7. **Model predicts spindle collapse in the absence of interdigitated MTs.** (A) Schematic representation of wt and *ase1Δ* models in which spindle force generation is turned off. (B) Simulation of mitotic progression and Kt dynamics in the *ase1* model. Red, SPBs; green, merotelic Kt. The spindle force generator is turned off at the 80-s time point.

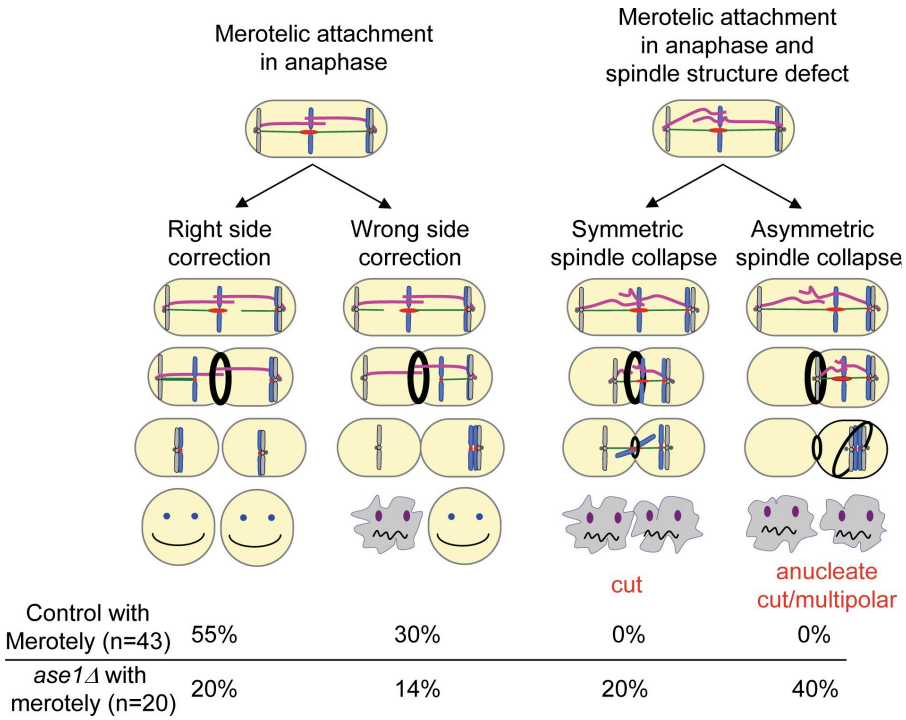

Control with Merotely (n=43)	55%	30%	0%	0%
ase1Δ with merotely (n=20)	20%	14%	20%	40%

Figure 8. **Model summarizing the different effects of merotelic attachment on mitotic progression.** Schematic representation illustrating the impact of merotelic attachment in control cells (left) and in cells with a defective spindle structure (right). In the control cells, the correction of merotelic attachment is coordinated with the onset of cytokinesis to avoid the formation of cut/anucleate. In cells with a defective spindle structure (*ase1* mutant), this coordination is lost, leading to the appearance of a cut/anucleate phenotype and cell death. The different categories of cells were scored by live cell imaging using either a *rad21-K1 ndc80-gfp cdc11-cfp myo2-gfp* strain or an *ase1Δ rad21-K1 ndc80-gfp cdc11-cfp myo2-gfp* during mitosis from metaphase to cytokinesis and cell abscission. For clarity, the model does not include the percentage of cells showing merotelic Kt disruption (15% for control and 6% for *ase1Δ*).

such a model is far from being established because the biochemical constants involved in MT dynamics within the Kt sleeve are unknown. We chose a macroscopic approach to study the biological mechanics at the Kt. In our model, the Kt is seen as an object that can move MTs either forward or backward. All of the undefined biochemical constants are described by a single force applied to the Kt. The model faithfully reproduces the in vivo observations, including Kt stretching, relaxation, and correction. It confirms that in the presence of merotelic attachment, the spindle is constrained by simple mechanical links. This simple model could also explain the phenotype of spindle collapse recently reported in several fission yeast mutants (Alexandru et al., 2001; Griffiths et al., 2008). The model also predicts that the bias seen toward correction, and not random segregation, is likely to be the consequence of a different number of MTs linking the merotelic Kt to the two SPBs (e.g., three MTs to one SPB and one to the other). The molecular mechanisms that explain this bias are unknown. A more general mitotic model that takes into account the state of attachment of all the Kts (merotelic or synthelic) from metaphase to anaphase needs to be established. Comparison of such a model and observed Kt dynamics in wt and mutant strains will highlight the mechanisms of MT dynamics at the Kt that promote successful biorientation.

In fission yeast, the spindle is positioned in the middle of the cell and is encircled by an actin ring that is detectable early in metaphase (Arai and Mabuchi, 2002; Wu et al., 2003). During anaphase B, spindle structure is stabilized by the presence of overlapping antiparallel MTs (Ding et al., 1993), the destruction of which results in the collapse of the mitotic apparatus when a merotelic Kt is present. This can either happen symmetrically or asymmetrically in respect to the actomyosin ring, leading to a cut phenotype or to the formation of aneuploid cells after completion of cytokinesis. In our mathematical model, asymmetric collapse is a consequence of a different number of MTs linking the merotelic Kt to the two SPBs (see previous paragraph), but we cannot exclude the possibility that astral MTs may also play a role in anchoring one of the two poles to the cell cortex (Gachet et al., 2004; Tolić-Nørrelykke et al., 2004). In budding yeast, the kinesin Kar3 provides, like Ase1, the structural stability of the spindle in the presence of a dicentric chromosome (Gardner et al., 2008). We found no such role for Klp2 (Kar3 homologue; unpublished data), although this kinesin has been implicated in Kt capture by MTs in both yeasts (Tanaka et al., 2007; Gachet et al., 2008). The function of Kar3 in budding yeast during dicentric attachment could be explained by a role for this kinesin in chromosome cohesion (Mayer et al., 2004) rather than at the interdigitated MT midzone. Alternatively, because in the case of a dicentric chromosome the forces are applied on the chromosome arms in between the two dicentric chromosomes rather than on the Kt structure itself, it is possible that the motor proteins involved in dicentric chromosome stretching or merotelic Kt stretching are different.

In conclusion, our study provides a unique biological model illustrating the impact of merotelic attachment on mitotic progression, starting from metaphase to anaphase up to the execution of cytokinesis. Our findings suggest that a disbalance of forces exerted by MTs on the merotelic Kt create a brute force mechanism that is essential for the correction of merotelic attachments in anaphase. When the structure of the spindle is affected, merotelic attachments are not corrected, and cells undergo asymmetric division or cut phenotype, leading to cell death (Fig. 8). This mechanism is likely to be conserved in higher eukaryotes, as our mathematical model is simply based on force balance generated by molecular motors characterized by linear force–velocity relationships. Additionally, Ase1 (Prc1) is evolutionarily conserved, and correction of merotelic attachment is known to be

a key process in maintaining genomic stability in eukaryotic cells. Knowing that asymmetric cell division has in the past only been attributed to defects in spindle positioning, our work opens a new field of investigation in this domain.

Materials and methods

Cell culture

Media, growth, maintenance of strains, and genetic methods were performed as described previously by Moreno et al. (1991). *rad21-K1* mutant was provided by M. Yanagida (Kyoto University, Kyoto, Japan), and *ase1* mutant was provided by P. Tran (Institut Curie, Paris, France). Cells were grown at 25°C (Fig. S4) in yeast extract and centrifuged for 30 s at 3,000 *g* before mounting onto an imaging chamber. The different strains used in this study are listed in Table S1.

Cell fixation

To determine the percentage of aneuploidy and cut phenotype, cells were fixed in 3.7% formaldehyde for 7 min at room temperature, washed once in PBS, and observed in the presence of DAPI/calcofluor.

Live cell imaging

Live cell analysis was performed in an imaging chamber (CoverWell PCI-2.5; Grace Bio-Laboratories) filled with 1 ml 1% agarose in minimal medium and sealed with a 22 × 22–mm glass coverslip. Time-lapse images of z stacks (maximum of five stacks of 0.3–0.4-µm steps to avoid photobleaching) were taken at 15-s intervals at 25°C. Exposure times were 300–500 ms using a light source (HIGHlite; Roper Industries) reduced to 30% to avoid phototoxicity and photobleaching. Either the image with the best focal plane or projected images was prepared for each time point. Images were visualized with a charge-coupled device camera (CoolSNAP HQ; Roper Industries) fitted to an upright microscope (DM6000; Leica) with a 100× or 63× 1.4 NA objective and SEMROCK filters for GFP, CFP, or RFP and were recorded using the MetaMorph software package (MDS Analytical Technologies). Intensity adjustments (threshold adjustments) were made using the MetaMorph, ImageJ (National Institutes of Health), and Photoshop (Adobe) packages. MetaMorph was used to create line scans.

Analysis of Kt dynamics

The position of the SPBs and Kts was determined by the visualization of the Ndc80–GFP and Cdc11–CFP signals and was captured using MetaMorph. Maximum intensity projections were prepared for each time point, with the images from each channel being combined into a single RGB image. These images were cropped around the cell of interest, and optional contrast enhancement was performed in MetaMorph where necessary. The cropped images were exported to IGOR (version Pro6; http://www.wavemetrics.com) as 8-bit RGB-stacked TIFF files, with each frame corresponding to one image of the time-lapse series. For both channels, custom peak detection was performed. The successive positions of the SPBs and Kts were determined, and eventual detection errors were manually corrected. The data generated were used to calculate the mean speed at which the Kts reached the SPBs, the rate of spindle elongation, the rate of spindle retraction, and the number of Kts at the SPBs. A stretched merotelic Kt is defined as a single Kt within an anaphase spindle (i.e., all of the other Kts have permanently regained the poles), which undergoes splitting and separates by at least 0.5 µm.

Laser ablation of mitotic cells

The system used to perform laser ablation is composed of a conventional inverted microscope (DMI6000B; Leica) equipped with a heated stage and covered with an incubation system including a temperature controller. Mitotic spindle photo ablation was achieved with a frequency-doubled Nd:YAG-pulsed laser at a wavelength of 532 nm; the pulse was estimated to have a duration of 600 ps with a repetition rate of 10 kHz (532-nm Sealed Green Microchip; JDS Uniphase). The guiding of the beam was performed using an L5D head (Roper Industries) coupled to the microscope through the epifluorescence port. In brief, the L5D head constituted of a laser shutter and a galvanometer pair mirror that guides the laser beam within the field of view of the camera. The beam is focused with a 100× NA 1.4 Plan Apo oil immersion objective lens (HCS; Leica). Images were acquired with a cooled charge-coupled device camera (CoolSNAP HQ2). The system is driven by MetaMorph software.

Mathematical model of merotelic attachment

The mathematical model used in this study is essentially an adaptation and a simplification of the framework developed by Civelekoglu-Scholey et al. (2006). Indeed, merotelic attachment at anaphase only differs from proper attachment in metaphase in that the pair of sister chromatids linked by chromatin is replaced by two sides of the Kt linked by the Kt structure.

In our model, the mitotic spindle is described as a one-dimensional organization of $2N + 2$ elements, where N is the number of merotelic Kts: $2N$ Kt sides and two poles. All of the positions are given with respect to an axis with its origin at the spindle center. In the following, the positions of the top and bottom poles are denoted as x_s and x_s^*, respectively. By definition of the coordinate system, $x_s^* = -x_s \; \forall t$. Speeds are denoted as $\dot{x}_s$ and $\dot{x}_s^*$. Similarly, the positions of the n^{th} Kt sides are denoted as x_n and x_n^*, and their speeds are denoted as $\dot{x}_n$ and $\dot{x}_n^*$, respectively, for the top and bottom sides of chromosome n with $n \in [1, N]$. At each time, the number of kt–MTs plugged to the top and bottom Kt sides of chromosome n is denoted as M_n and M_n^*.

Force balance model

Three interactions are considered: (1) the structural link between $\dot{x}_s$ the two sides of the Kt, represented by a damped oscillator (Fig. 7 B), (2) an attractive force linking the spindle pole and its respective attachment site, and (3) the spindle elongation force, pushing poles outward.

Although the actual centromere structure is composed of multiple layers and different materials, we assume for the sake of simplicity that it can be described as the combination of a spring of stiffness κ and rest length d_0 and a dashpot of friction coefficient μ_k. Elastic to plastic transition (Marko, 2008), as observed during stretching, is accounted for by a critical length d_c over which the material breaks, with κ and μ_k being set to 0. The first force, exerted by the centromeric material on the Kt top attachment site is thus expressed by

$$F_n^c = -\kappa\left(x_n - x_n^* - d_0\right) - \mu_k\left(\dot{x}_n - \dot{x}_n^*\right). \tag{1}$$

Civelekoglu-Scholey et al. (2006) and Cheeseman and Desai (2008) assume that Kt movement is the result of a combination of molecular motors and polymerization/depolymerization of the Kt MTs. Polymerizing (Kolomeisky and Fisher, 2001) and depolymerizing MTs coupled to the Kts (McIntosh et al., 2008) and molecular motors (Toba et al., 2006) can be faithfully described by a linear force–velocity relationship. Considering the net force linking the Kt attachment site and the pole as a linear combination of those force generators, it can also be described as a force–velocity relationship. We hypothesize that this force is always directed toward the spindle pole:

$$F_n^k = M_n(t) F_k \left(1 - \frac{\dot{x}_n - \dot{x}_s}{V_k}\right), \tag{2}$$

$$F_n^{k*} = -M_n^{k*}(t) F_k \left(1 - \frac{\dot{x}_s^* - \dot{x}_n^*}{V_k}\right), \tag{3}$$

$$= M_n^*(t) F_k \left(1 + \frac{\dot{x}_s + \dot{x}_n^*}{V_k}\right). \tag{4}$$

F_k and V_k are the stall force and the maximum speed, respectively, for the Kt–spindle pole interaction. Motor proteins and cross-linkers attach to the overlap between interpolar MTs. Those elements are considered to exert an overall outward force on the SPBs, which again is described by a force–velocity relationship:

$$F_{idz} = F_{mz}\left(1 - \frac{\dot{x}_s - \dot{x}_s^*}{V_{mz}}\right), \tag{5}$$

$$= F_{mz}\left(1 - \frac{2\dot{x}_s}{V_{mz}}\right), \tag{6}$$

$$F_{idz*} = -F_{idz}. \tag{7}$$

The stall force F_{mz} and maximum speed V_{mz} are considered constant throughout the simulation, assuming that the structure and function of the midzone does not change during the cycle.

In the highly viscous nucleoplasm, inertia can be neglected with respect to drag force. Eqs. 1–7 can thus be combined in the following set of coupled first order differential equations:

$$\mu_k \dot{x}_n = F_n^k + F_n^c, \tag{8}$$

$$\mu_k \dot{x}_n^* = F_n^{k*} - F_n^c, \tag{9}$$

$$\mu_s \dot{x}_s = F_{idz} - \sum_n^N F_n^k, \text{ and} \tag{10}$$

$$\mu_s \dot{x}_s^* = -F_{idz} - \sum_n^N F_n^{k*} = -\mu_s \dot{x}_s. \tag{11}$$

Kt–MT attachment

During mitosis, dynamic instability of MTs is highly regulated, and, as already described in *Saccharomyces cerevisiae* (Gardner et al., 2005), polymerization and depolymerization rates may vary within the spindle. A rigorous molecular or mesoscopic description of MT dynamics is thus a problem on its own, and published models often require numerous parameters. MT–Kt interaction strength might depend on molecular motor-binding rates, MT penetration depth in the Kt structure (Joglekar and Hunt, 2002), and other factors such as length-dependent regulations. In our model, we account for MT behavior by the factor M_n in the Kt–spindle pole interaction. We only account for MT dynamic instability as attachment and detachment stochastic events. That is, at each time step, attached kt–MTs have a probability P_d to detach, and unattached kt–MTs have a probability P_a to attach. These probabilities are characterized by attachment and detachment frequencies f_a and f_d, respectively, and the time interval dt between two steps, according to a Poisson distribution:

$$P_d = 1 - \exp(-f_d\, dt) \quad P_a = 1 - \exp(-f_a\, dt). \tag{12}$$

In this study, we assume that those frequencies are constants.

Parameter setting

The system of Eqs. 8–12 is first expressed in dimensionless quantities, with V_k as the unit of speed and F_k as the unit of force, and 1 µm and 1 s as the units of length and time, respectively. The remaining parameters were chosen to fit with the experimental measurements as depicted in Fig. 6. Those parameters are kept constant for all the simulations unless specified otherwise. In the case of Kt disruption, the Kt–MT force generators will work near their maximum velocity, with friction being small compared with those forces. The maximum velocity V_k will thus be slightly higher than the maximum observed poleward speed of the Kt fragment. To comply with direct experimental measurement of this speed, V_k is thus set to 0.03 µm/s. We cannot directly quantify the force exerted by the MTs at the Kt. Yet, the literature suggests that this must be on the order of 10 *pN* for a single MT. Thus, we chose $F_{max}^k = 10\,pN$ to estimate the magnitudes of the other parameters (Table I). The values of the friction coefficients of the Kt and SPB are higher than reported elsewhere (Nicklas, 1988) by about a factor of 10. This discrepancy comes essentially from the relative roughness of the dynamic instability description. A higher friction coefficient allows smoothing out of the abrupt, nonphysiological changes induced by the plugged/unplugged events, thus capturing the more gentle changes, such as single motor association to or dissociation from MT.

Numerical solution

The system is solved numerically using Python (version 2.5) with the Numpy (version 1.1.0) and Scipy (version 0.6.0) packages among others. The system is initialized with random position and attachment of the merotelic Kts and with a fixed spindle length. At each time step, a random number between 0 and 1 is first attributed to each MT from a uniform distribution. For attached and unattached MTs, if this number is inferior to P_a (attached) or P_e (unattached), the MT detaches or attaches, respectively. The position-dependent forces are calculated, and the algebraic system of equations is solved using the linear algebra PACKage. The position of each element is updated according to the resulting speeds. It is possible to simulate several events: (1) chromatid elastic to plastic transition; if the distance between the two attachment sites exceeds a critical size (1.6 µm according to experimental measurements), the spring constant is set to 0, allowing the two sites to move freely toward the poles. (2) A laser can be simulated; in this case, the link between a Kt side and its respective pole is broken. (3) In the system, this corresponds to setting F_k and F_{idz} to 0. (4) *ase1Δ* strains are simulated by setting F_{idz} to 0 at a given spindle critical length (L = 7 µm; Tanaka et al., 2007; this study).

Online supplemental material

Fig. S1 shows that stretched merotelic Kts are single chromatids and show simultaneous laser ablation of cells within the same field. Fig. S2 shows kymographs of multiple merotelic attachments. Figs. S3 and S4 show that merotelic attachment leads to cut/asymmetric division/multipolar spindles and cell death in the absence of Ase1. Fig. S5 shows simulations of multiple merotelic attachments and of a reduction in the spindle force generator during spindle elongation. Videos 1 and 2 show time-lapse imaging of wt or *rad21-K1* with both Kt and SPB signals imaged simultaneously. Video 3 shows time-lapse imaging of laser ablation of a merotelic attachment. Videos 4 and 5 show time-lapse imaging of *ase1Δ* or *ase1Δ rad21-K1* cells expressing SV40-GFP-atb2 as a marker of α-tubulin (spindle) and Ndc80-GFP as a marker of the Kts. Videos 6–9 show time-lapse imaging of wt, *rad21-K1*, or *ase1Δ rad21-K1* (Videos 8 and 9) cells with the actomyosin ring, with the Kts and the SPBs imaged simultaneously. Table S1 lists the *S. pombe* strains used in this study. Online supplemental material is available at http://www.jcb.org/cgi/content/full/jcb.200902093/DC1.

We thank T. Toda, P. Tran, K. Hardwick, J. Millar, R. McIntosh, M. Yanagida, and J.P. Javerzat for supplying strains, J. Hyams for his support and critical reading of the manuscript, T. Toda, Y. Watanabe, J.P. Javerzat, A. Merdes, and F. Payre for helpful discussions, Corinne Lorenzo for assistance with microscopy, and B. Ducommun and the members of the Laboratoire de Biologie Cellulaire et Moléculaire du Controle de la Prolifération for their support.

T. Courtheoux is supported by a fellowship from La Ligue contre le cancer. G. Gay is supported by the Centre National de la Recherche Scientifique. The microscopy equipment was funded by the Centre National de la Recherche Scientifique, l'Université de Toulouse, l'Association de la Recherche sur le Cancer, and GlaxoSmithKline.

Submitted: 18 February 2009
Accepted: 7 October 2009

References

Alexandru, G., F. Uhlmann, K. Mechtler, M.A. Poupart, and K. Nasmyth. 2001. Phosphorylation of the cohesin subunit Scc1 by Polo/Cdc5 kinase regulates sister chromatid separation in yeast. *Cell.* 105:459–472. doi:10.1016/S0092-8674(01)00362-2

Andrews, P.D., Y. Ovechkina, N. Morrice, M. Wagenbach, K. Duncan, L. Wordeman, and J.R. Swedlow. 2004. Aurora B regulates MCAK at the mitotic centromere. *Dev. Cell.* 6:253–268. doi:10.1016/S1534-5807(04)00025-5

Arai, R., and I. Mabuchi. 2002. F-actin ring formation and the role of F-actin cables in the fission yeast *Schizosaccharomyces pombe*. *J. Cell Sci.* 115:887–898.

Botvinick, E.L., V. Venugopalan, J.V. Shah, L.H. Liaw, and M.W. Berns. 2004. Controlled ablation of microtubules using a picosecond laser. *Biophys. J.* 87:4203–4212. doi:10.1529/biophysj.104.049528

Brust-Mascher, I., G. Civelekoglu-Scholey, M. Kwon, A. Mogilner, and J.M. Scholey. 2004. Model for anaphase B: role of three mitotic motors in a switch from poleward flux to spindle elongation. *Proc. Natl. Acad. Sci. USA.* 101:15938–15943. doi:10.1073/pnas.0407044101

Cahill, D.P., C. Lengauer, J. Yu, G.J. Riggins, J.K. Willson, S.D. Markowitz, K.W. Kinzler, and B. Vogelstein. 1998. Mutations of mitotic checkpoint genes in human cancers. *Nature.* 392:300–303. doi:10.1038/32688

Cheeseman, I.M., and A. Desai. 2008. Molecular architecture of the kinetochore-microtubule interface. *Nat. Rev. Mol. Cell Biol.* 9:33–46. doi:10.1038/nrm2310

Choi, S.H., M.P. Peli-Gulli, I. McLeod, A. Sarkeshik, J.R. Yates III, V. Simanis, and D. McCollum. 2009. Phosphorylation state defines discrete roles for monopolin in chromosome attachment and spindle elongation. *Curr. Biol.* 19:985–995.

Cimini, D., B. Howell, P. Maddox, A. Khodjakov, F. Degrassi, and E.D. Salmon. 2001. Merotelic kinetochore orientation is a major mechanism of aneuploidy in mitotic mammalian tissue cells. *J. Cell Biol.* 153:517–527. doi:10.1083/jcb.153.3.517

Cimini, D., B. Moree, J.C. Canman, and E.D. Salmon. 2003. Merotelic kinetochore orientation occurs frequently during early mitosis in mammalian tissue cells and error correction is achieved by two different mechanisms. *J. Cell Sci.* 116:4213–4225. doi:10.1242/jcs.00716

Cimini, D., L.A. Cameron, and E.D. Salmon. 2004. Anaphase spindle mechanics prevent mis-segregation of merotelically oriented chromosomes. *Curr. Biol.* 14:2149–2155. doi:10.1016/j.cub.2004.11.029

Cimini, D., X. Wan, C.B. Hirel, and E.D. Salmon. 2006. Aurora kinase promotes turnover of kinetochore microtubules to reduce chromosome segregation errors. *Curr. Biol.* 16:1711–1718. doi:10.1016/j.cub.2006.07.022

Civelekoglu-Scholey, G., D.J. Sharp, A. Mogilner, and J.M. Scholey. 2006. Model of chromosome motility in *Drosophila* embryos: adaptation of a general mechanism for rapid mitosis. *Biophys. J.* 90:3966–3982. doi:10.1529/biophysj.105.078691

Cleveland, D.W., Y. Mao, and K.F. Sullivan. 2003. Centromeres and kinetochores: from epigenetics to mitotic checkpoint signaling. *Cell.* 112:407–421. doi:10.1016/S0092-8674(03)00115-6

Courtheoux, T., G. Gay, C. Reyes, S. Goldstone, Y. Gachet, and S. Tournier. 2007. Dynein participates in chromosome segregation in fission yeast. *Biol. Cell.* 99:627–637. doi:10.1042/BC20070047

Ding, R., K.L. McDonald, and J.R. McIntosh. 1993. Three-dimensional reconstruction and analysis of mitotic spindles from the yeast, *Schizosaccharomyces pombe*. *J. Cell Biol.* 120:141–151. doi:10.1083/jcb.120.1.141

Gachet, Y., S. Tournier, J.B. Millar, and J.S. Hyams. 2004. Mechanism controlling perpendicular alignment of the spindle to the axis of cell division in fission yeast. *EMBO J.* 23:1289–1300. doi:10.1038/sj.emboj.7600156

Gachet, Y., C. Reyes, T. Courthéoux, S. Goldstone, G. Gay, C. Serrurier, and S. Tournier. 2008. Sister kinetochore recapture in fission yeast occurs by two distinct mechanisms, both requiring Dam1 and Klp2. *Mol. Biol. Cell.* 19:1646–1662. doi:10.1091/mbc.E07-09-0910

Ganem, N.J., S.A. Godinho, and D. Pellman. 2009. A mechanism linking extra centrosomes to chromosomal instability. *Nature.* 460:278–282.

Gardner, M.K., and D.J. Odde. 2006. Modeling of chromosome motility during mitosis. *Curr. Opin. Cell Biol.* 18:639–647. doi:10.1016/j.ceb.2006.10.006

Gardner, M.K., C.G. Pearson, B.L. Sprague, T.R. Zarzar, K. Bloom, E.D. Salmon, and D.J. Odde. 2005. Tension-dependent regulation of microtubule dynamics at kinetochores can explain metaphase congression in yeast. *Mol. Biol. Cell.* 16:3764–3775. doi:10.1091/mbc.E05-04-0275

Gardner, M.K., J. Haase, K. Mythreye, J.N. Molk, M. Anderson, A.P. Joglekar, E.T. O'Toole, M. Winey, E.D. Salmon, D.J. Odde, and K. Bloom. 2008. The microtubule-based motor Kar3 and plus end–binding protein Bim1 provide structural support for the anaphase spindle. *J. Cell Biol.* 180:91–100. doi:10.1083/jcb.200710164

Gregan, J., C.G. Riedel, A.L. Pidoux, Y. Katou, C. Rumpf, A. Schleiffer, S.E. Kearsey, K. Shirahige, R.C. Allshire, and K. Nasmyth. 2007. The kinetochore proteins Pcs1 and Mde4 and heterochromatin are required to prevent merotelic orientation. *Curr. Biol.* 17:1190–1200. doi:10.1016/j.cub.2007.06.044

Griffiths, K., H. Masuda, S. Dhut, and T. Toda. 2008. Fission yeast dam1-A8 mutant is resistant to and rescued by an anti-microtubule agent. *Biochem. Biophys. Res. Commun.* 368:670–676. doi:10.1016/j.bbrc.2008.01.156

Heald, R., R. Tournebize, T. Blank, R. Sandaltzopoulos, P. Becker, A. Hyman, and E. Karsenti. 1996. Self-organization of microtubules into bipolar spindles around artificial chromosomes in *Xenopus* egg extracts. *Nature.* 382:420–425. doi:10.1038/382420a0

Joglekar, A.P., and A.J. Hunt. 2002. A simple, mechanistic model for directional instability during mitotic chromosome movements. *Biophys. J.* 83:42–58. doi:10.1016/S0006-3495(02)75148-5

Kenney, R.D., and R. Heald. 2006. Essential roles for cohesin in kinetochore and spindle function in *Xenopus* egg extracts. *J. Cell Sci.* 119:5057–5066. doi:10.1242/jcs.03277

Khodjakov, A., R.W. Cole, B.F. McEwen, K.F. Buttle, and C.L. Rieder. 1997. Chromosome fragments possessing only one kinetochore can congress to the spindle equator. *J. Cell Biol.* 136:229–240. doi:10.1083/jcb.136.2.229

Kolomeisky, A.B., and M.E. Fisher. 2001. Force-velocity relation for growing microtubules. *Biophys. J.* 80:149–154. doi:10.1016/S0006-3495(01)76002-X

Loïodice, I., J. Staub, T.G. Setty, N.P. Nguyen, A. Paoletti, and P.T. Tran. 2005. Ase1p organizes antiparallel microtubule arrays during interphase and mitosis in fission yeast. *Mol. Biol. Cell.* 16:1756–1768. doi:10.1091/mbc.E04-10-0899

Mallavarapu, A., K. Sawin, and T. Mitchison. 1999. A switch in microtubule dynamics at the onset of anaphase B in the mitotic spindle of *Schizosaccharomyces pombe*. *Curr. Biol.* 9:1423–1426. doi:10.1016/S0960-9822(00)80090-1

Maresca, T.J., and E.D. Salmon. 2009. Intrakinetochore stretch is associated with changes in kinetochore phosphorylation and spindle assembly checkpoint activity. *J. Cell Biol.* 184:373–381. doi:10.1083/jcb.200808130

Marko, J.F. 2008. Micromechanical studies of mitotic chromosomes. *Chromosome Res.* 16:469–497. doi:10.1007/s10577-008-1233-7

Mayer, M.L., I. Pot, M. Chang, H. Xu, V. Aneliunas, T. Kwok, R. Newitt, R. Aebersold, C. Boone, G.W. Brown, and P. Hieter. 2004. Identification of protein complexes required for efficient sister chromatid cohesion. *Mol. Biol. Cell.* 15:1736–1745. doi:10.1091/mbc.E03-08-0619

McIntosh, J.R., E.L. Grishchuk, M.K. Morphew, A.K. Efremov, K. Zhudenkov, V.A. Volkov, I.M. Cheeseman, A. Desai, D.N. Mastronarde, and F.I. Ataullakhanov. 2008. Fibrils connect microtubule tips with kinetochores: a mechanism to couple tubulin dynamics to chromosome motion. *Cell.* 135:322–333. doi:10.1016/j.cell.2008.08.038

Mogilner, A., R. Wollman, G. Civelekoglu-Scholey, and J. Scholey. 2006. Modeling mitosis. *Trends Cell Biol.* 16:88–96. doi:10.1016/j.tcb.2005.12.007

Moreno, S., A. Klar, and P. Nurse. 1991. Molecular genetic analysis of fission yeast *Schizosaccharomyces pombe*. *Methods Enzymol.* 194:795–823. doi:10.1016/0076-6879(91)94059-L

Mulvihill, D.P., C. Barretto, and J.S. Hyams. 2001. Localization of fission yeast type II myosin, Myo2, to the cytokinetic actin ring is regulated by phosphorylation of a C-terminal coiled-coil domain and requires a functional septation initiation network. *Mol. Biol. Cell.* 12:4044–4053.

Nasmyth, K., and A. Schleiffer. 2004. From a single double helix to paired double helices and back. *Philos. Trans. R. Soc. Lond. B Biol. Sci.* 359:99–108. doi:10.1098/rstb.2003.1417

Nicklas, R.B. 1988. The forces that move chromosomes in mitosis. *Annu. Rev. Biophys. Biophys. Chem.* 17:431–449. doi:10.1146/annurev.bb.17.060188.002243

Norden, C., M. Mendoza, J. Dobbelaere, C.V. Kotwaliwale, S. Biggins, and Y. Barral. 2006. The NoCut pathway links completion of cytokinesis to spindle midzone function to prevent chromosome breakage. *Cell.* 125:85–98. doi:10.1016/j.cell.2006.01.045

O'Toole, E.T., M. Winey, and J.R. McIntosh. 1999. High-voltage electron tomography of spindle pole bodies and early mitotic spindles in the yeast *Saccharomyces cerevisiae*. *Mol. Biol. Cell.* 10:2017–2031.

Pellman, D., M. Bagget, Y.H. Tu, G.R. Fink, and H. Tu. 1995. Two microtubule-associated proteins required for anaphase spindle movement in *Saccharomyces cerevisiae*. *J. Cell Biol.* 130:1373–1385. doi:10.1083/jcb.130.6.1373

Pidoux, A.L., S. Uzawa, P.E. Perry, W.Z. Cande, and R.C. Allshire. 2000. Live analysis of lagging chromosomes during anaphase and their effect on spindle elongation rate in fission yeast. *J. Cell Sci.* 113:4177–4191.

Sakuno, T., K. Tada, and Y. Watanabe. 2009. Kinetochore geometry defined by cohesion within the centromere. *Nature.* 458:852–858. doi:10.1038/nature07876

Samejima, I., T. Matsumoto, Y. Nakaseko, D. Beach, and M. Yanagida. 1993. Identification of seven new cut genes involved in *Schizosaccharomyces pombe* mitosis. *J. Cell Sci.* 105:135–143.

Tanaka, T.U., N. Rachidi, C. Janke, G. Pereira, M. Galova, E. Schiebel, M.J. Stark, and K. Nasmyth. 2002. Evidence that the Ipl1-Sli15 (Aurora kinase-INCENP) complex promotes chromosome bi-orientation by altering kinetochore-spindle pole connections. *Cell.* 108:317–329. doi:10.1016/S0092-8674(02)00633-5

Tanaka, K., E. Kitamura, Y. Kitamura, and T.U. Tanaka. 2007. Molecular mechanisms of microtubule-dependent kinetochore transport toward spindle poles. *J. Cell Biol.* 178:269–281. doi:10.1083/jcb.200702141

Tatebayashi, K., J. Kato, and H. Ikeda. 1998. Isolation of a *Schizosaccharomyces pombe* rad21ts mutant that is aberrant in chromosome segregation, microtubule function, DNA repair and sensitive to hydroxyurea: possible involvement of Rad21 in ubiquitin-mediated proteolysis. *Genetics.* 148:49–57.

Thompson, S.L., and D.A. Compton. 2008. Examining the link between chromosomal instability and aneuploidy in human cells. *J. Cell Biol.* 180:665–672. doi:10.1083/jcb.200712029

Tighe, A., V.L. Johnson, M. Albertella, and S.S. Taylor. 2001. Aneuploid colon cancer cells have a robust spindle checkpoint. *EMBO Rep.* 2:609–614. doi:10.1093/embo-reports/kve127

Toba, S., T.M. Watanabe, L. Yamaguchi-Okimoto, Y.Y. Toyoshima, and H. Higuchi. 2006. Overlapping hand-over-hand mechanism of single molecular motility of cytoplasmic dynein. *Proc. Natl. Acad. Sci. USA.* 103:5741–5745. doi:10.1073/pnas.0508511103

Tolić-Nørrelykke, I.M., L. Sacconi, G. Thon, and F.S. Pavone. 2004. Positioning and elongation of the fission yeast spindle by microtubule-based pushing. *Curr. Biol.* 14:1181–1186. doi:10.1016/j.cub.2004.06.029

Tomonaga, T., K. Nagao, Y. Kawasaki, K. Furuya, A. Murakami, J. Morishita, T. Yuasa, T. Sutani, S.E. Kearsey, F. Uhlmann, et al. 2000. Characterization of fission yeast cohesin: essential anaphase proteolysis

of Rad21 phosphorylated in the S phase. *Genes Dev.* 14:2757–2770. doi:10.1101/gad.832000

Tournier, S., Y. Gachet, V. Buck, J.S. Hyams, and J.B. Millar. 2004. Disruption of astral microtubule contact with the cell cortex activates a Bub1, Bub3, and Mad3-dependent checkpoint in fission yeast. *Mol. Biol. Cell.* 15:3345–3356. doi:10.1091/mbc.E04-03-0256

Toyoda, Y., K. Furuya, G. Goshima, K. Nagao, K. Takahashi, and M. Yanagida. 2002. Requirement of chromatid cohesion proteins rad21/scc1 and mis4/scc2 for normal spindle-kinetochore interaction in fission yeast. *Curr. Biol.* 12:347–358. doi:10.1016/S0960-9822(02)00692-9

Uchida, K.S., K. Takagaki, K. Kumada, Y. Hirayama, T. Noda, and T. Hirota. 2009. Kinetochore stretching inactivates the spindle assembly checkpoint. *J. Cell Biol.* 184:383–390. doi:10.1083/jcb.200811028

Uhlmann, F., F. Lottspeich, and K. Nasmyth. 1999. Sister-chromatid separation at anaphase onset is promoted by cleavage of the cohesin subunit Scc1. *Nature.* 400:37–42. doi:10.1038/21831

Wise, D.A., and B.R. Brinkley. 1997. Mitosis in cells with unreplicated genomes (MUGs): spindle assembly and behavior of centromere fragments. *Cell Motil. Cytoskeleton.* 36:291–302. doi:10.1002/(SICI)1097-0169(1997)36:3<291::AID-CM9>3.0.CO;2-A

Wu, J.Q., J.R. Kuhn, D.R. Kovar, and T.D. Pollard. 2003. Spatial and temporal pathway for assembly and constriction of the contractile ring in fission yeast cytokinesis. *Dev. Cell.* 5:723–734. doi:10.1016/S1534-5807(03)00324-1

Yamashita, A., M. Sato, A. Fujita, M. Yamamoto, and T. Toda. 2005. The roles of fission yeast ase1 in mitotic cell division, meiotic nuclear oscillation, and cytokinesis checkpoint signaling. *Mol. Biol. Cell.* 16:1378–1395. doi:10.1091/mbc.E04-10-0859

Yanagida, M. 1998. Fission yeast cut mutations revisited: control of anaphase. *Trends Cell Biol.* 8:144–149. doi:10.1016/S0962-8924(98)01236-7

Yokobayashi, S., M. Yamamoto, and Y. Watanabe. 2003. Cohesins determine the attachment manner of kinetochores to spindle microtubules at meiosis I in fission yeast. *Mol. Cell. Biol.* 23:3965–3973. doi:10.1128/MCB.23.11.3965-3973.2003